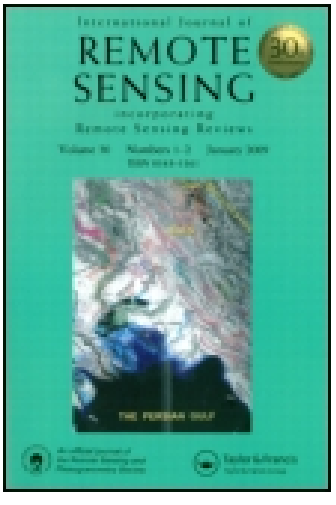

International Journal of Remote Sensing

Publication details, including instructions for authors and subscription information:
http://www.tandfonline.com/loi/tres20

A resource limited artificial immune system algorithm for supervised classification of multi/hyper-spectral remote sensing imagery

L. Zhang [a] , Y. Zhong [a] , B. Huang [b] & P. Li [a]

[a] The State Key Laboratory of Information Engineering in Surveying, Mapping and Remote Sensing , Wuhan University , People's Republic of China

[b] Department of Geography and Resource Management , The Chinese University of Hong Kong Shatin , NT , Hong Kong and Institute of Remote Sensing Applications , Chinese Academy of Sciences , Beijing

Published online: 05 Apr 2007.

To cite this article: L. Zhang , Y. Zhong , B. Huang & P. Li (2007) A resource limited artificial immune system algorithm for supervised classification of multi/hyper-spectral remote sensing imagery, International Journal of Remote Sensing, 28:7, 1665-1686, DOI: 10.1080/01431160600675903

To link to this article: http://dx.doi.org/10.1080/01431160600675903

International Journal of Remote Sensing
Vol. 28, No. 7, 10 April 2007, 1665–1686

Taylor & Francis
Taylor & Francis Group

A resource limited artificial immune system algorithm for supervised classification of multi/hyper-spectral remote sensing imagery

L. ZHANG†, Y. ZHONG†, B. HUANG*‡ and P. LI†

†The State Key Laboratory of Information Engineering in Surveying, Mapping and Remote Sensing, Wuhan University, People's Republic of China

‡Department of Geography and Resource Management, The Chinese University of Hong Kong Shatin, NT, Hong Kong and Institute of Remote Sensing Applications, Chinese Academy of Sciences, Beijing

(*Received 13 August 2005; in final form 6 March 2006*)

The resource limited artificial immune system (RLAIS), a new computational intelligence approach, is being increasingly recognized as one of the most competitive methods for data clustering and analysis. Nevertheless, owing to the inherent complexity of the conventional RLAIS algorithm, its application to multi/hyper-class remote sensing image classification has been considerably limited. This paper explores a novel artificial immune algorithm based on the resource limited principles for supervised multi/hyper-spectral image classification. Three experiments with different types of images were performed to evaluate the performance of the proposed algorithm in comparison with other traditional image classification algorithms: parallelepiped, minimum distance, maximum likelihood, K-nearest neighbour and back-propagation neural network. The results show that the proposed algorithm consistently outperforms the traditional algorithms in all the experiments and hence provides an effective new option for processing multi/hyper spectral remote sensing images.

1. Introduction

Artificial immune systems (AIS) have recently drawn increased attention from the artificial intelligence community. AIS were inspired by the human immune system and have been exploited in a wide spectrum of applications (Dasgupta 1999, De Castro and Timmis 2002). Some application examples include pattern recognition (Carter 2000, Tarakanov and Skormin 2002), intrusion detection (Forrest *et al.* 1994, Kim and Bentley 2001), clustering (Timmis *et al.* 2000, 2001), and optimization (De Castro and Von Zuben 2002). In particular, a novel immune model, namely resource limited artificial immune system (RLAIS) (Timmis *et al.* 2000, 2001), has been devised for data analysis and clustering using a population control mechanism. Based on this model, an artificial immune recognition system (AIR) for general purpose supervised classification was developed (Watkins and Boggess 2002).

*Corresponding author. Email: huang@geomatics.ucalgary.ca

International Journal of Remote Sensing
ISSN 0143-1161 print/ISSN 1366-5901 online © 2007 Taylor & Francis
http://www.tandf.co.uk/journals
DOI: 10.1080/01431160600675903

Despite the successful applications of AIS, RLAIS, and AIR in several domains, only few applications have been reported in the area of remote sensing (Zhang *et al.* 2004). This may be attributed to the high computational costs associated with the original AIS algorithm, thus rendering it unsuitable for remote sensing image classification. The huge volume of multi/hyper-spectral remote sensing image data may be another impediment. To overcome these problems, this study develops a novel algorithm based on RLAIS for supervised multi/hyper-spectral remote sensing image classification.

Classification is a fundamental issue in image processing, and various supervised algorithms, such as parallelepiped (PP), minimum distance (MD), maximum likelihood (ML) and K-nearest neighbour (K-NN) have been developed in the past several decades for classifying multi/hyper-spectral data in a pixel-wise manner (Campbell 2002, Landgrebe 2002). The PP classifier (Campbell 2002), also known as box decision rule, is probably the simplest among the above-mentioned algorithms. This algorithm relies on the ranges of values within the training data to define regions within a multidimensional data space. The MD classifier (Duda *et al.* 2001) uses the central values of the spectral data that form the training dataset to assign pixels to information categories. The K-NN algorithm (Campbell 2002) assumes that pixels close to each other in the feature space are likely to fall in the same class. It then assigns the classification of the majority vote among the K nearest neighbours in the training samples to the pixel in question. The familiar ML classifier is a powerful classification technique based on the maximum likelihood decision rule. The rule assumes that both the training data and the classes themselves usually present multivariate normal frequency distributions (Campbell 2002). To improve on the classification performance, several new classifiers have also been devised for multi/hyper-spectral remote sensing image classification such as artificial neural networks (Heermann and Khazenie 1992, Carpenter *et al.* 1997), genetic algorithms (Tso and Mather 1999) and support vector machines (Melgani and Bruzzone 2004).

Unlike the aforementioned classification algorithms, the proposed algorithm based on RLAIS is a robust self-learning algorithm. In particular, the algorithm is novel in the following aspects:

a. It is a data driven self-adaptive method and can thus adjust itself to the data without any explicit specification of functional or distributional form for the underlying model.
b. It is viewed as a universal functional approximator since it can approximate any function through arbitrary accuracy.
c. It utilizes an immune model making it flexible in modelling real world complex relationships through immunological properties, such as memory property and clonal selection.

The proposed algorithm, when examined with various multi/hyper-spectral images, demonstrates high classification accuracy, thus providing a new option for multi/hyper-spectral remote sensing image classification.

The rest of the paper is structured as follows. Section 2 gives an overview of the human immune system and resource limited AIS. Section 3 details the proposed method and algorithm, while section 4 illustrates the performance of the proposed algorithm compared with the traditional algorithms. Section 5 analyses the sensitivity of the proposed algorithm in relation to its main parameters. Finally, section 6 concludes the paper.

2. Resource limited artificial immune system (RLAIS)

2.1 *Human immune system*

The human immune system is a complex system made up of cells, molecules and organs that together constitute an identification mechanism capable of perceiving and combating dysfunction from our own cells and the action of exogenous infectious micro-organisms as well. The human immune system safeguards us against infectious agents such as viruses, bacteria, fungi, and other parasites. Any molecule that can be recognized by the adaptive immune system is known as an antigen. Lymphocytes or the white blood cells are the fundamental components of the immune system. Within the human body, lymphocytes are found in two forms, B cells and T cells. Functionally, these two types of cells differ in their mode of antigen recognition. B-cells are capable of recognizing antigens free in solution, while T cells require antigens to be presented by other accessory cells. Each has its distinct chemical structure and produces many Y-shaped antibodies from its surface to kill the antigens. Antibodies are molecules attached primarily to the surface of B cells whose aim is to recognize and bind to antigens (Jerne 1973).

The immune system possesses several properties such as self/non-self discrimination immunological memory, positive/negative selection, immunological network, clonal selection and learning which performs complex tasks. In particular, immunological memory is the ability of the adaptive immune system to mount a more effective immune response against antigen after its first encounter, leaving the body better able to resist in the future (Timmis *et al.* 2001).

2.2 *RLAIS*

RLAIS is modelled primarily on the mechanisms of the B-cells in the biological immune system. The RLAIS exhibits behaviour such that once a strong pattern has been identified the network will not deteriorate or lose the pattern (Timmis *et al.* 2000, 2001). RLAIS was proposed not only for clustering as one shot learning, but also for the system to perform continuous learning.

Antigens in RLAIS are instantiated as feature vectors that are presented to the system during training and testing. Table 1 summarizes the mapping between the immune system and RLAIS. In particular, RLAIS adopts the concept of artificial recognition balls (ARBs). Each ARB can be thought of as a representation of numerous B-cells, all of which have the same antibody. ARBs, otherwise known as resources, are limited to a finite number and are responsible for the primary memory mechanism in the immune system. When ARBs are cloned, they must undergo

Table 1. Mapping between the immune system and RLAIS.

Immune system	RLAIS
Antibody	Feature vector
Recognition ball	Combination of feature vector and vector class
Shape-space	The possible values of the data vector
Clonal expansion	Reproduction of ARBs that are well matched with antigens
Antigens	Training data
Affinity maturation	Random mutation of ARB and removal of lowest stimulated ARBs
Immune memory	Memory set of mutated ARBs
Metadynamics	Continual removal and creation of ARBs and memory cells

affinity mutation inversely proportional to the antigenic affinity: the higher the affinity, the smaller the mutation rate. The term metadynamics of the immune system refers to the continuous change of the ARB population through antibodies proliferation and death. The above process is embedded in RLAIS with the continual creation and removal of antibodies with lower affinity from the population.

A key issue for applying AIS to classification is related to the development of the memory cell pool. RLAIS has the ability to limit the size of the memory cell pool to develop the memory cell population which will be further used to classify test instances.

In a RLAIS, the training of an antigen, Ag, and the processing of each ARB are conducted through a resource allocation mechanism according to the stimulation level between the ARB and Ag. It is assumed that the whole resource of RLAIS is fixed or set by users. ARBs are stimulated through a response to an invading antigen. After exposure to a given antigen (or antigen population), each ARB attempts to consume resources based on its stimulation level. However, since the numbers of resources are finite, only the most stimulated ARBs will actually consume resources. The remaining ARBs (i.e. those without resources) are removed from the system. This competition for resources applies a certain amount of evolutionary pressure to ensure that only the strongest ARBs (i.e. those most adept at recognizing antigens) remain in the system.

The regulating process of RLAIS is that we calculate the average stimulation for each ARB, and check for the termination condition. If the average stimulation value of each ARB class group is less than a given threshold, the process will continue. In the above process, the system resources are allocated to a given ARB based on its normalized stimulation value, which is also used as an indication of its affinity being a recognizer of the training antigen. If the resource of ARB is more than the allowable threshold, the worst antibody with the lowest stimulation in ARB will be continuously removed until the resource decreases to the allowable range (Watkins and Boggess 2002).

3. Resource-limited classification of remote sensing image (RLCRSI)

In RLAIS, the stimulation value of an ARB and the distribution of resources are based on the class of the ARB, which increases the complexity of the system. However, if the regions of interest or samples are selected humanly from a remote sensing image or a spectral library, each region of interest or sample can be represented as an individual class. Thus, maintaining class diversity is not necessary in this case. Based on RLAIS, the resources are only allocated to ARBs of the same class as the antigen and in proportion to the inverse of an ARB's affinity to the antigen. As a result, the computational cost of the corresponding algorithm decreases without sacrificing the classification accuracy.

In the proposed algorithm, RLCRSI, the stopping criterion of the training process no longer takes into account the stimulation value of ARBs in all classes, but only accounts for the stimulation value of the ARBs of the same class as the antigen. This will not affect the stopping criterion since the changes to the proposed algorithm now only require that the average stimulation value of the ARBs of the same class as the antigen be above the stimulation threshold.

The above process is illustrated in figure 1 by a simple example in two-dimensional feature space. At first, a training antigen is presented to the ARB in the

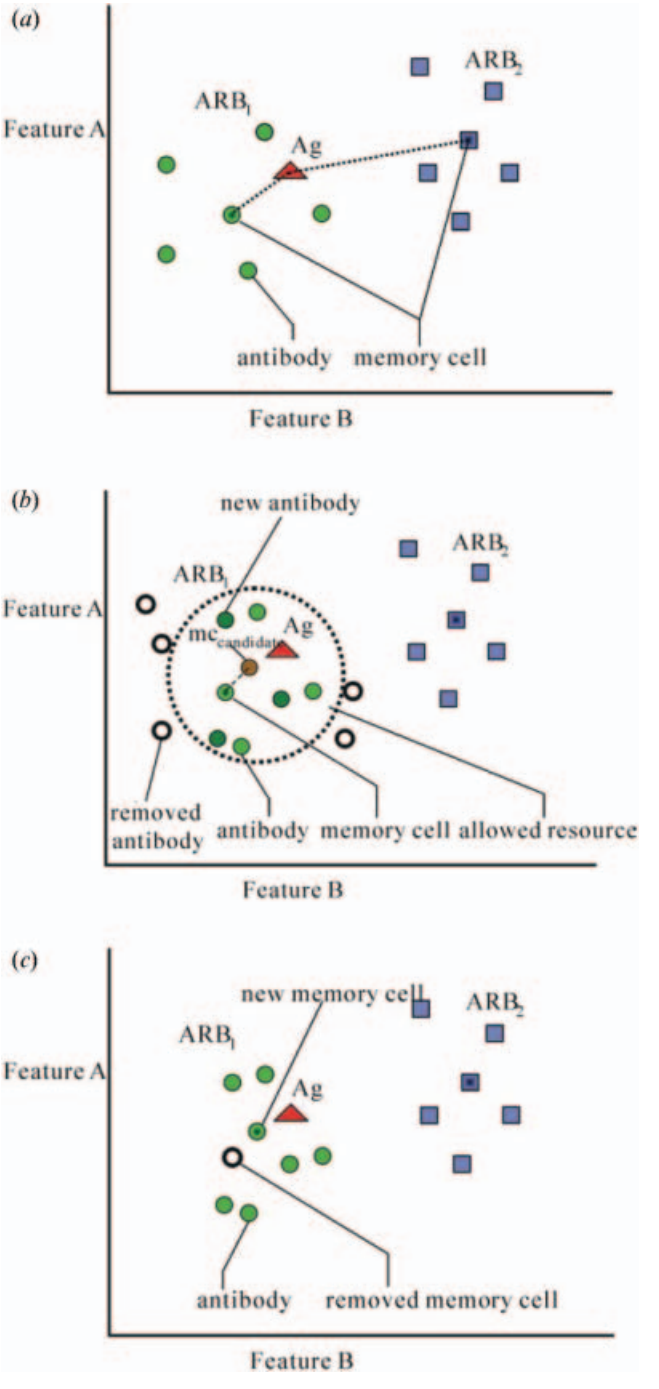

Figure 1. The principle of RLCRSI. (*a*) ARB selected, (*b*) the memory cell clones and mutates, producing new antibody and a candidate memory cell (antibodies with lower stimulation level are removed), (*c*) ARB pool is evolved.

same class as the antigen (figure 1 (*a*)). In the ARB, once the memory cell with the highest stimulation level to the antigen is then sufficiently stimulated and rapidly produces clones of itself. Meanwhile, the clones undergo a mutation process at particular sites in its gene to produce new antibodies. Each antibody must compete for a fixed amount of resources: if the resources of any antibody are out of the allowable range, it will be removed from the ARB pool (figure 1 (*b*)). The highest stimulation antibody is selected as a candidate memory cell, $mc_{\text{candidate}}$, to evolve the memory cell, which is able to match the antigen more closely (figure 1 (*c*)). The evolved memory cells will be used for the classification.

The implementation of RLCRSI includes the following six steps:

1. Selection of the regions of interest or samples.
2. Normalization and initialization.
3. ARB generation.
4. Competition for resources and nomination of candidate memory cells.
5. Promotion of candidate memory cells into memory cell pool. Through the five steps above, the memory cells are selected and used to classify a multi/hyper-spectral remote sensing image into step 6).
6. Classification.

These steps are detailed as follows:

3.1 *Selection of regions of interest or samples*

Based on the characteristics of the remote sensing image (e.g., texture, pixel's grey level) and application purposes, regions of interest or samples can be selected from an image or a spectral library.

3.2 *Normalization and initialization*

All feature vectors are firstly normalized such that the distances between antigens and ARBs or between two ARBs are in the range [0, 1]. Secondly, calculate the affinity threshold, which will be used to determine whether a new memory cell is close enough to an existing memory cell to replace it. For training sets of fixed size, the affinity threshold (AT) is the average affinity, which is calculated pair-wise over all training instances. If the training set is considered as antigens, the affinity threshold is calculated as:

$$AT = \frac{\sum_{i=1}^{n-1} \sum_{j=i+1}^{n} affinity(ag_i, ag_j)}{n(n-1)/2} \tag{1}$$

where n is the number of training data items, ag_i and ag_j are the ith and jth training antigen respectively, and *affinity* (x, y) returns the Euclidean distance between the two antigens feature vectors. The final step in initialization is the seeding of the memory cells and initial ARB population. This is performed by randomly choosing training antigens to be added to the set of memory cells and to the set of ARBs.

3.3 *ARB generation*

After initialization is completed, the next step is the identification of memory cells and ARB generations. Given a specific training antigen, *ag*, find the memory cell,

mc_{match}, which has the same class as the antigen and is most stimulated by the antigen. The formula for the identification of the memory cell is given as follows:

$$mc_{match} = \arg\max_{mc \in MC_{ag.c}} stimulation(ag, mc) \tag{2}$$

where *stimulation* (x, y) is defined as:

$$stimulation(x, y) = 1 - Affinity(x, y) \tag{3}$$

$$Affinity(x, y) = Euclidean\_dis\tan ce(x, y) = \sqrt{\sum_{i=1}^{bm} (x_i - y_i)^2} \tag{4}$$

where bm=the band number of the remote sensing image.

Once the memory cell with highest stimulation, mc_{match}, is identified, it generates new ARBs to place into the population of pre-existing ARBs. The algorithm creates *NClones*, which are new clones of mc_{match}. Each feature of the clone can be mutated with probability mutation_rate. *NClones* is defined as:

$$NClones = hyper\_clonal\_rate^{*} clonal\_rate^{*} stimulation(ag, mc_{match}) \tag{5}$$

where the *hyper_clonal_rate* and *clonal_rate* are integer values set by the user. The *clonal_rate* is used to determine how many clones are produced by ARBs and memory cells. Its typical value is 10. The *hyper_clonal_rate* is a multiplier which ensures that a hyper-mutating memory cell produce more new cells than a standard ARB.

3.4 *Competition for resources and development of a candidate memory cell,* $mc_{\text{candidate}}$

Let AB represent the set of ARBs and *ab* represent a single ARB, $ab \in$ AB. At this point, a set of ARBs which include mc_{match}, mutations from mc_{match}, and remnant ARBs from responses to previously encountered antigens is already generated. The detailed training procedure is described as follows:

3.4.1 Normalizing ARBs stimulation level and calculating the resources.

1. Firstly, find the maximum stimulation and minimum stimulation among all the ARBs.
2. For each $ab \in$ AB, normalize its stimulation according to equation (6):

$$ab.stim = \frac{ab.stim - \min stim}{\max stim - \min stim} \tag{6}$$

3. For each $ab \in$ AB, calculate ab's resources based on its stimulation level as follows:

$$ab.resources = ab.stim^{*} clonal\_rate \tag{7}$$

4. Metadynamics of ARBs. Sum all the resources of ARBs and named them as resAlloc. If this allocation of resources results in more resources being allocated across the population than allowed, then resources are removed from the weakest ARBs until the total number of resources in the system

returns to the number of resources allowed. Those ARBs with zero resources are removed from the ARB population.

3.4.2 Stopping criterion for the training procedure. Calculate the average stimulation level. If the average stimulation value of each ARB class group is less than a given stimulation threshold, the process moves to step 3.4.3, otherwise, jump to step 3.4.5.

3.4.3 Clonal expansion and affinity maturation. For each $ab \in$ AB, allow each ARB in AB the opportunity to produce mutated offspring. Clone and mutate a randomly selected subset of the ARBs based on the proportion to their stimulation level. The number of Clones, named *NClones*, is defined as:

$$NClones = clonal\_rate^{*} stimulation(ag, mc_{match}) \tag{8}$$

During the course of mutation, the higher the stimulation, the smaller the mutation rate. The mutation procedure and the corresponding function mutate(x) are defined in figure 2.

In figure 2, the function Irandom() returns a random value using a uniform distribution within the range [0,1] and Lrandom also returns a random value but using a uniform distribution within the range [−1,1]. As the evolutional process is described in real space, the mutation operation uses the non-uniform operator, which is able to achieve fine local tuning (Michalewicz 1992). The mutation function $\Delta(t, y)$ is defined as follows:

$$\Delta(t, y) = y\left(1 - r^{\left(1-\frac{t}{T}\right)^{\lambda}}\right) \tag{9}$$

where t is the iteration number; T, the maximum of iteration number; r, a random value in the range [0,1]; λ, a parameter to decide the nonconforming degree.

3.4.4 Re-judging stopping criterion. Calculate the average stimulation level. If the average stimulation value of each ARB class group is less than a given stimulation threshold, the process repeats from 3.4.1.until the stopping criterion is met.

```
mutate(x)
{
   for each(x.vi in x.v)
   do
        ai = minvi
        bi = maxvi
        rd_mr = Irandom()
        rd_to = Lrandom()
        if(rd_mr < mutation_rate)
           if(rd_to >= 0 )
              x.vi =   x.vi + Δ(t, bi - x.vi )
           else
              x.vi =   x.vi - Δ(t, x.vi - ai )
   done
   return x
}
```

Figure 2. Mutation.

3.4.5 Developing the candidate memory cell, $mc_{\text{candidate}}$. Select the highest affinity ARB of the same class as the antigen from the last antigenic interaction, as the candidate memory cell, $mc_{\text{candidate}}$.

3.5 *Promoting candidate memory cell to memory cell pool*

The final stage in the training process is the potential introduction of the just-developed candidate memory cell, $mc_{\text{candidate}}$, into the set of existing memory cells, MC. It is during this stage that the affinity threshold calculated during initialization becomes critical as it dictates whether the $mc_{\text{candidate}}$ will replace mc_{match} that was previously identified. The candidate memory cell is added to the set of memory cells only if it is more stimulated by the training antigen, ag, than mc_{match}, where stimulation is defined as in equation (3). If this test is passed, and if the affinity between $mc_{\text{candidate}}$ and mc_{match} is lesser than the product of the affinity threshold and the user-defined affinity threshold scalar (ATS), then $mc_{\text{candidate}}$ shall replace mc_{match} in the set of memory cells.

Once the candidate memory cell has been evaluated and added into the set of established memory cells, training on this particular antigen is completed. The next antigen in the training set, regions of interest, is then selected and the training process proceeds from step 3.3 to step 3.5. This process continues until all antigens in all regions of interest have been trained in the proposed algorithm.

3.6 *Classification*

After training is completed, the evolved memory cells are available for classification. The classification is performed in a K-NN search approach. Each memory cell is presented with a data item for stimulation. The system's classification of each data item is determined, using a majority vote of the outputs of the k most stimulated memory cells.

The flowchart for RLCRSI is shown in figure 3.

4. Experiments and analyses

The proposed RLCRSI and the traditional supervised algorithms were all implemented using Visual C^{++} 6.0 and tested on different types of images. Three experiments were carried out to test the performance of the RLCRSI algorithm, of which the main running parameters are clonal_rate, hyper_clonal_rate, mutation_rate, stimulation_threshold, the total number of resources (TotalNumResource), and affinity threshold scalar (ATS). Consistent comparisons were also carried out between RLCRSI and PP (parallelepiped), MD (minimum distance), ML (maximum likelihood), K-nearest neighbor (K-NN), and back-propagation neural network (BP) in all the experiments.

4.1 *Experiment 1: TM image*

To begin with, an experiment was performed using a 30-metre resolution multispectral Landsat TM image (400×400 pixels) of the Wuhan city acquired on 26 October 1998 (figure 4). The following four classes were used: water, vegetation, road and building. Four regions of interests (ROI) representing the four classes, respectively were selected as training regions and each training region had ground reference sample points. Figure 5 shows the spectra of the four training regions. The list of classes and the number of labelled samples for each class are given in table 2.

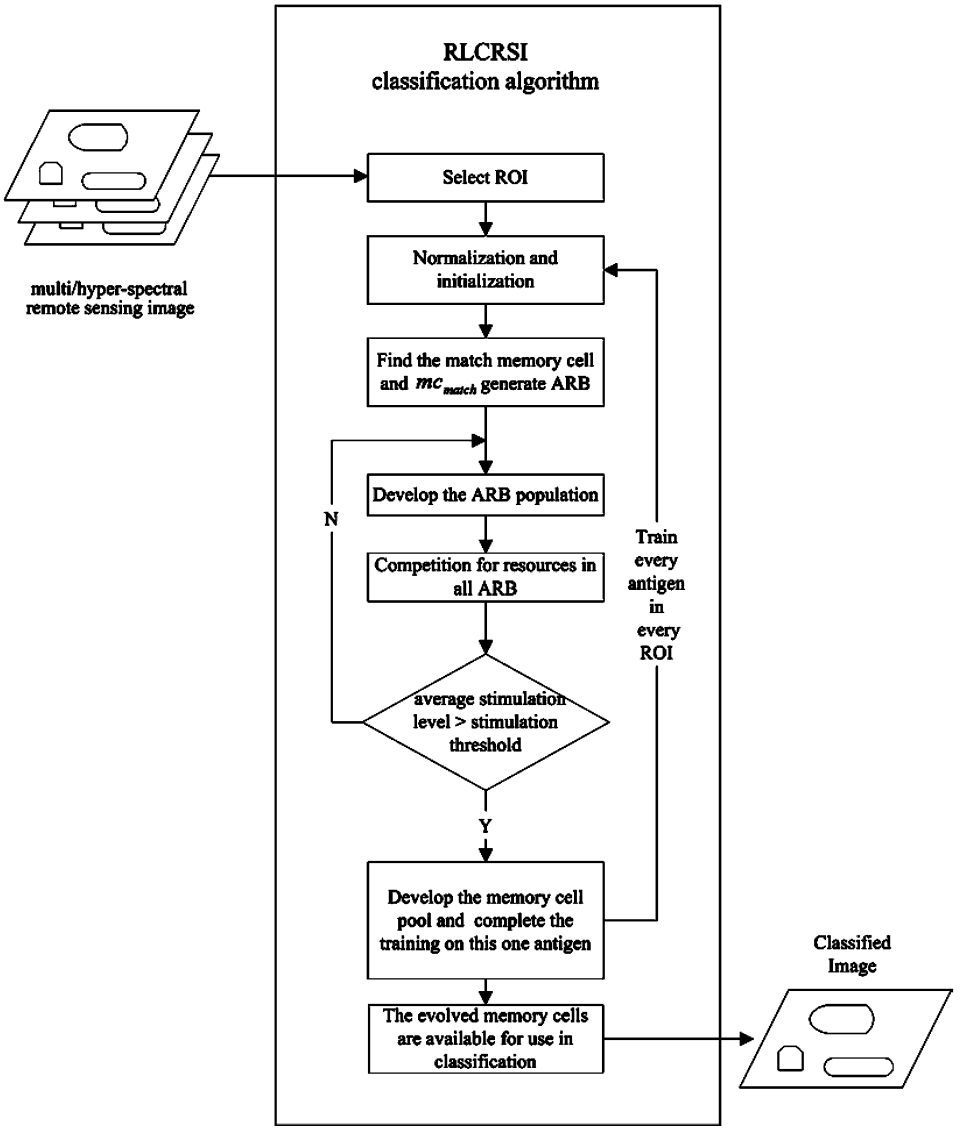

Figure 3. Flowchart for RLCRSI.

In this experiment, 17-NN was used and the number of hidden nodes and the learning rate in BP (using 1 hidden layer) were respectively, 20 and 0.25. The main parameters of RLCRSI were set as follows: clonal_rate=10, hyper_clonal_rate=2, mutation_rate=0.1, stimulation_threshold=0.9, TotalNumResource=50, and ATS=0.8.

Figure 6 (*a*)–(*f*) illustrates the classification results using RLCRSI and other algorithms, respectively. To evaluate the classification accuracy, a test field map was provided in figure 6(*g*) based on the ground truth data.

The visual comparisons of the six supervised classifications in figure 6 show varying degrees of pixel assignment accuracy. The six classifiers generate similar classification results in the water class. Still, it is hard for PP to differentiate among

Figure 4. Wuhan TM image RGB (3, 2, 1).

other classes and many unknown pixels (black pixels) exist in its classified image (figure 6(*b*)). Although MD and K-NN can recognize buildings and roads, they cannot distinguish the vegetation class. ML can make a distinction of vegetation from other classes; however, it surprisingly misclassified the water pixels in the right of the image to the building class. Furthermore, BP is competent in the classification though some building pixels are misclassified to vegetation. Nevertheless, RLCRSI

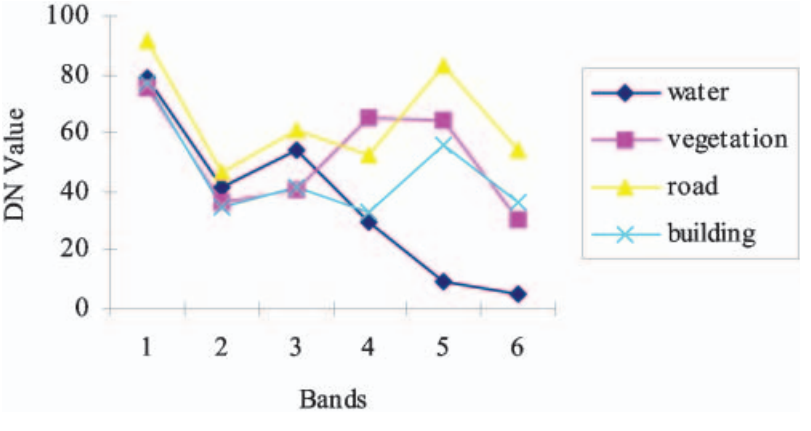

Figure 5. Spectra of four classes.

Table 2. List of classes and number of labelled samples in each class for experiment 1.

Class name	Number of labelled samples
Water	7090
Vegetation	6414
Road	7173
Building	6430
Total number of samples	27107

achieves the best visual accuracy in the vegetation class than other classifiers and also performs satisfactorily on the building and road classes.

Table 3 shows the comparison of RLCRSI with the five other classifiers in terms of overall accuracy, Kappa coefficient, and computation time. Clearly, RLCRSI

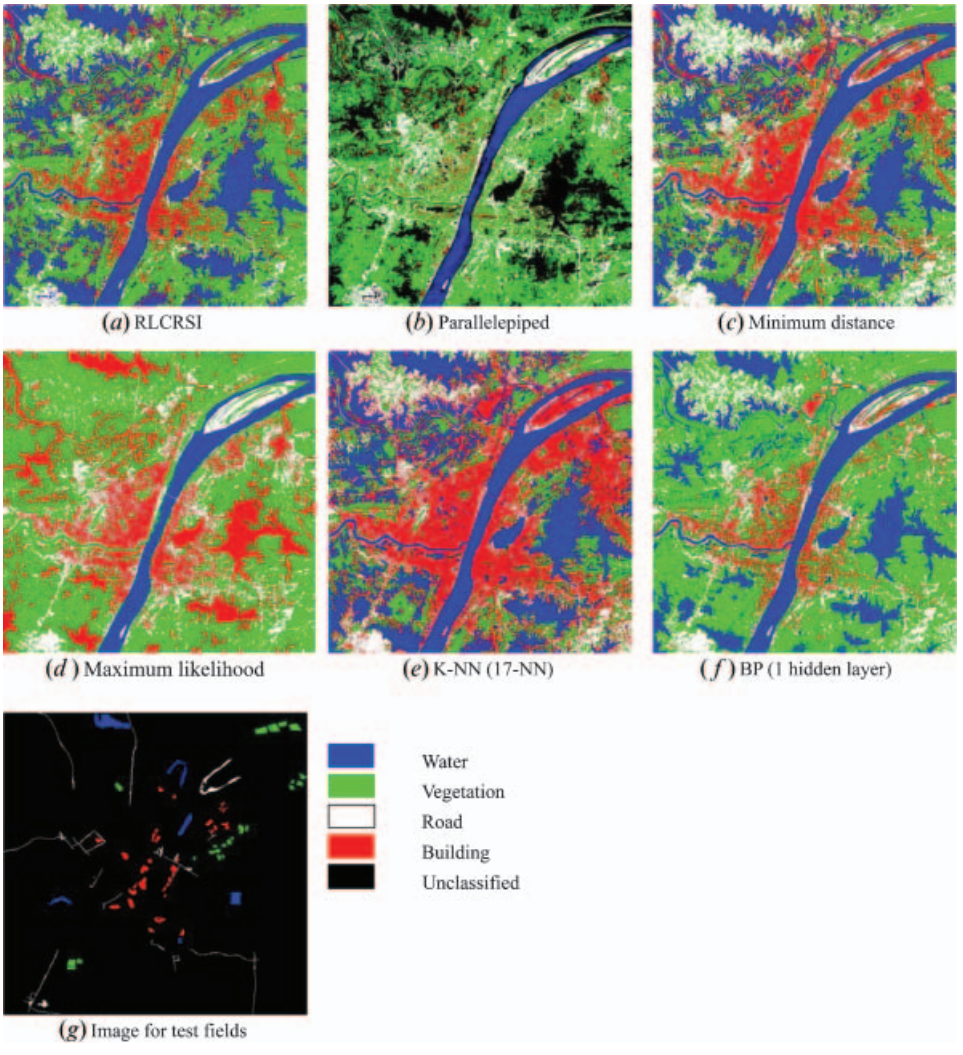

Figure 6. Supervised classification of Wuhan TM image.

Table 3. Comparison of RLCRSI with other algorithms in classifying the TM image.

Accuracy	Parallelepiped (PP)	Minimum distance (MD)	Maximum likelihood (ML)	K-NN (17-KNN)	BP (one hidden layer)	RLCRSI
Overall accuracy (%)	58.36	77.31	88.31	81.44	89.22	92.33
Kappa coefficient	0.5133	0.7213	0.8314	0.7867	0.8523	0.891
Time (s)	1.1	1.1	2.4	6.5	50.8	5.2

performs the best with the overall accuracy of 92.33% and Kappa coefficient of 0.891. This is followed by BP, ML, K-NN, MD and lastly, PP. Although the computation time of RLCRSI is higher than ML, it may be reduced by selecting the appropriate parameters. This will be investigated in our future work.

The comparatively high accuracy achieved by RLCRSI is attributed to the fact that ML assumes that both training data and the classes themselves present multivariate normal (Gaussian) frequency distributions (Campbell 2002). However, due to the complexity of ground substances and the diversity of disturbance, data from remotely sensed images often do not strictly adhere to this rule, thus leading to the relatively poor performance. BP and K-NN may achieve better accuracy; however they require much higher computational costs. BP's accuracy is significantly influenced by the training data. By contrast, RLCRSI is a kind of data driven self-adaptive method which can adjust itself to the data without any explicit specification of functional or distributional form for the underlying model. RLCRSI can approximate any function with arbitrary accuracy by a universal functional approximation. In addition, RLCRSI adopts an immune model rendering it flexible in modelling the complex relationships between classes. These enable RLCRSI to achieve the best accuracy.

4.2 *Experiment 2: MODIS image*

In this experiment, a MODIS image (acquired on 2 April 2002) of an area also in Wuhan was tested. The level 1B data sets include the 500 metre reflectance data for channels 3–7. These five spectral channels are ordered by ascending wavelengths at 0.46–0.48, 0.55–0.57, 1.63–1.65 and 2.11–2.16 μm, respectively. The classifications were performed using four regions of interest (ROI), namely water, cloud, city, and vegetation. Figure 7 shows the experimental MODIS image and figure 8 shows the spectra of the four training regions. The list of classes and the number of labelled samples for each class are given in table 4.

In the classification calculation, 17-NN was applied and the number of hidden nodes and the learning rate in BP (using 1 hidden layer) were respectively, 20 and 0.25. The parameters for RLCRSI were set as follows: clonal_rate=10, hyper_clonal _rate=2, mutation_rate=0.1, stimulation_threshold=0.85, TotalNumResource=50, and ATS=0.8.

Figure 9(*a*)–(*f*) illustrates the classification results using RLCRSI, PP, MD, ML, K-NN (17-NN), and BP (using one hidden layer), respectively. To evaluate the classification accuracy, a test field map was provided in figure 9(*g*) based on the ground truth data. The classification accuracy and CPU time for all the classifiers are given in table 5.

Figure 7. WUHAN MODIS image.

As shown in figure 9, RLCRSI achieves better visual results. By contrast, PP has many unclassified pixels; ML, MD and BP cannot recognize well the city class. In particular, MD misclassifies many pixels of other classes to the cloud class. K-NN and RLCRSI are more capable of differentiating the city class from other classes, whereas K-NN cannot distinguish the vegetation class which is misclassified to other classes. In addition, table 5 shows that the RLCRSI classifier produces better classifications than the traditional classifiers. RLCRSI improves the overall

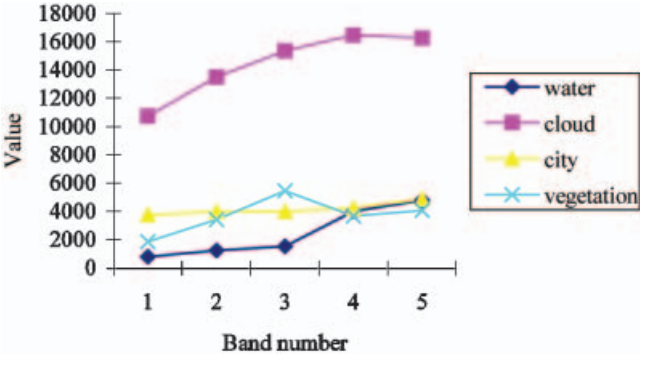

Figure 8. Spectral values of four classes.

Table 4. List of classes and number of labelled samples in each class for experiment 2.

Class name	Number of labelled samples
Water	2045
Vegetation	1149
City	1374
Cloud	1247
Total number of samples	5815

classification accuracy from 67.44% using PP to 93.67%, and the Kappa coefficient from 0.6122 to 0.91 with the reasonable computational time, 5.4 s. This shows that RLCRSI is a very competent classifier for remote sensing imagery.

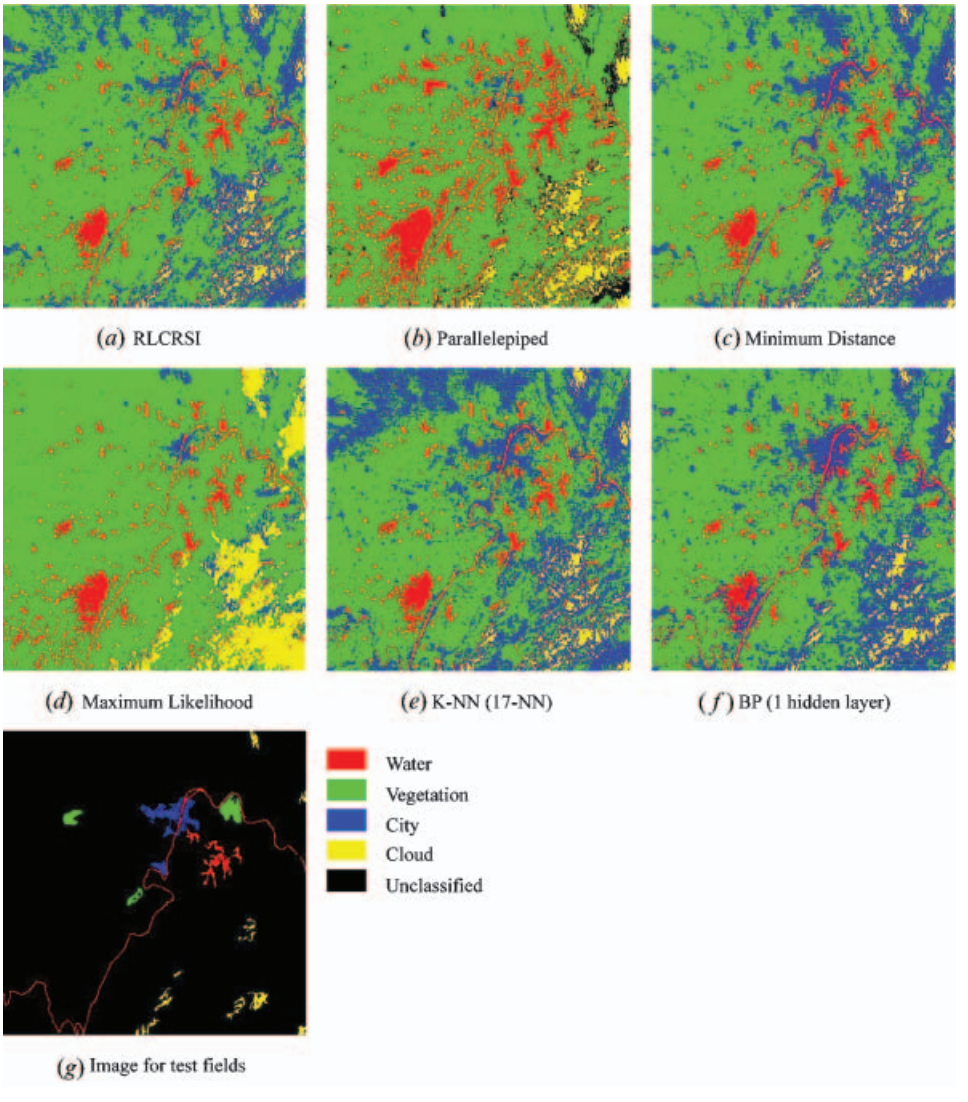

Figure 9. Supervised classification of Wuhan MODIS image.

Table 5. Comparison of RLCRSI with other algorithms in classifying the MODIS image.

Accuracy	Parallelepiped (PP)	Minimum distance (MD)	Maximum likelihood (ML)	K-NN (17-KNN)	BP (one hidden layer)	RLCRSI
Overall accuracy (%)	67.44	79.35	86.87	81.47	87.88	93.67
Kappa coefficient	0.6122	0.7343	0.8333	0.7767	0.8439	0.91
Time (s)	1.5	1.5	3.5	10.4	60	5.4

4.3 *Experiment 3: PHI image*

The data for this experiment was collected with an airborne imaging spectrometer (PHI) from the Xiaqiao test site, a mixed agricultural area. 80 bands of the PHI image (340×390 pixels) were utilized, and their spectral ranges were from 0.417 to 0.854 μm. The classification was performed using seven regions of interest. These regions representing the four classes respectively were selected as training regions. Figure 10 shows the PHI image and figure 11 shows the spectra profile of the seven training regions. The list of classes and the number of labelled samples for each class are given in table 6.

In this classification experiment, 17-NN was used and the number of hidden nodes and the learning rate in BP (using one hidden layer) were respectively, 30 and 0.25. The parameters for RLCRSI were defined as: clonal_rate=10, hyper_clonal_rate=2, mutation_rate=0.1, stimulation_threshold=0.85, TotalNumResource=50, and ATS=0.8.

Figure 12(*a*) illustrates the classification result using RLCRSI. Figures 12(*b*)–(*f*) illustrate the classification results using PP, MD, ML, K-NN (17-NN), and BP (using one hidden layer), respectively. To evaluate the classification accuracy, a test field map was also provided in figure 12(*g*) based on the ground truth data. The classification accuracy for the six classifiers is given in table 7.

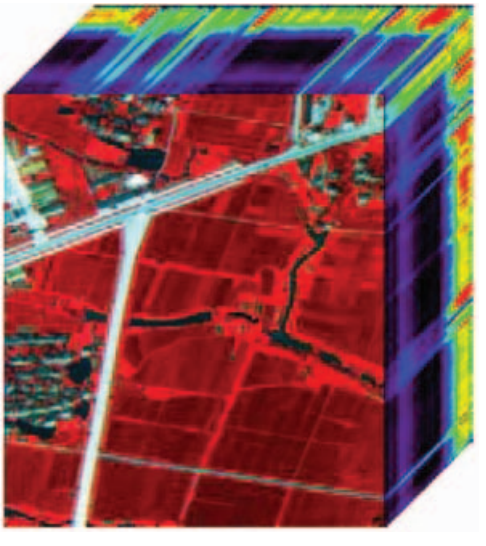

Figure 10. Xiaqiao PHI image.

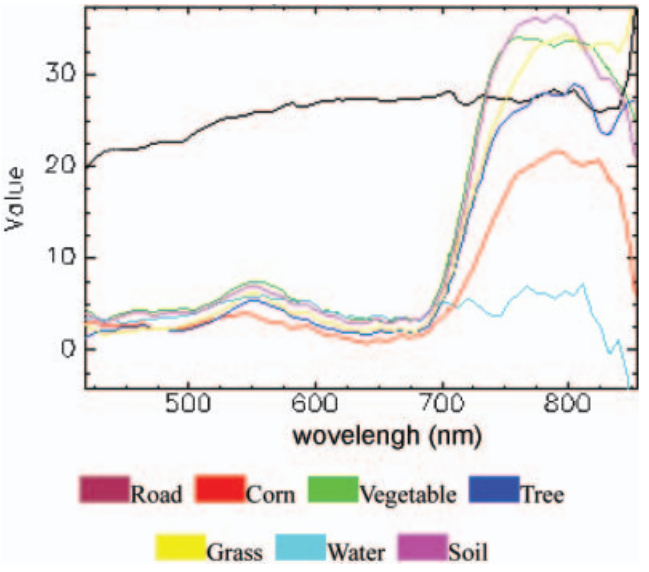

Figure 11. Spectra of the seven classes.

As shown in table 6, once again, RLCRSI achieves the highest overall accuracy and Kappa coefficient among the six classifiers. It improves the overall accuracy from 54.21% using PP to 90.15% (i.e. by 35.94%) and Kappa coefficient from 0.50 to 0.88 (i.e. by 0.38) with the satisfactory computational time, 15.5 s. This demonstrates that RLCRSI excels in hyper-spectral image classification.

5. Sensitivity analysis of RLCRSI

RLCRSI has three main user-defined parameters that significantly influence:

(i) the number of memory cells; and
(ii) the computational complexity of the algorithm:

- clonal_rate: the rate of clonal antibody,
- stimulation threshold: the stopping criterion for the training procedure,
- ATS: affinity threshold scalar which affects the number of memory cell population and computational.

Table 6. List of classes and number of labelled samples in each class for experiment 3.

Class name	Number of labelled samples
Road	716
Corn	1430
Vegetable	1030
Tree	263
Grass	255
Water	492
Soil	585
Total number of samples	4771

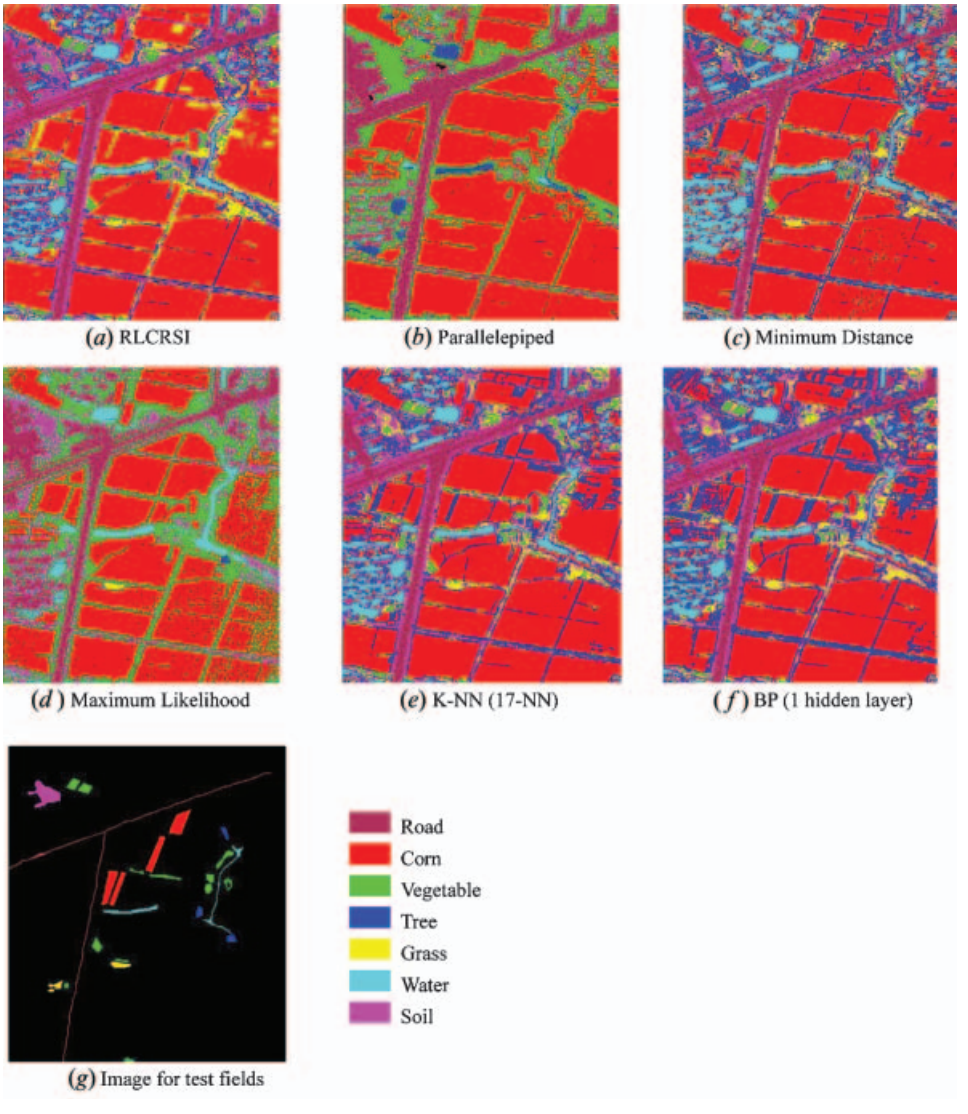

Figure 12. Supervised classification of XiaQiao PHI image.

Table 7. Comparison of RLCRSI with other algorithms in classifying the PHI image.

Accuracy	Parallelepiped (PP)	Minimum distance (MD)	Maximum likelihood (ML)	K-NN (17-KNN)	BP (one hidden layer)	RLCRSI
Overall accuracy (%)	54.21	78.62	86.13	80.31	86.63	90.15
Kappa coefficient	0.50	0.75	0.835	0.7897	0.8371	0.88
Time (s)	3.4	3.8	8.2	50.8	120.3	15.5

In order to analyse the effects of these parameters on RLCRSI, the Wuhan TM image, shown in figure 4, was classified using different parameter values.

5.1 *Sensitivity in relation to clonal_rate*

In order to study the RLCRSI sensitivity in relation to clonal_rate, other parameters were set as the same as those in experiment 1 and the clonal_rate was tested with the following values: clonal_rate={5, 10, 15, 20, 25, 35, 40, 50}.

Figure 13 shows that the higher the clonal_rate, the more the computation time. Particularly, when the clonal_rate increases from 10 to 50, the CPU time sharply increases from 5.2s to 61s while the overall accuracy of classification just shows slight improvement from 92.33% to 92.87%

5.2 *Sensitivity in relation to ATS*

Affinity threshold scalar (ATS) plays a very important role in maintaining the diversity of memory cell population and updating the memory cell population. In this test, the other parameters are maintained the same as in experiment 1 and ATS was assigned the following values: ATS={0, 0.1, 0.2, 0.3, 0.4, 0.5, 0.6, 0.7, 0.8, 0.9, 1}. As figure 14 shows, the number of memory cells decreases from 1523 to 4, while ATS increases from 0 to 1.0. The number of memory cells is the sum of the memory cells in each class.

It should be noted that when ATS=0.0, the memory cell population is the largest, leading to better classification results. However, more computational time is required. For large size remote sensing datasets, the appropriate value of ATS should be carefully selected. It is also interesting to observe that the number of memory cells is equal to the number of classes when ATS=1.0.

5.3 *Sensitivity in relation to stimulation threshold*

Stimulation threshold as a stopping criterion is closely related to the classification accuracy. Similar to the last test, other parameters were maintained the same as in

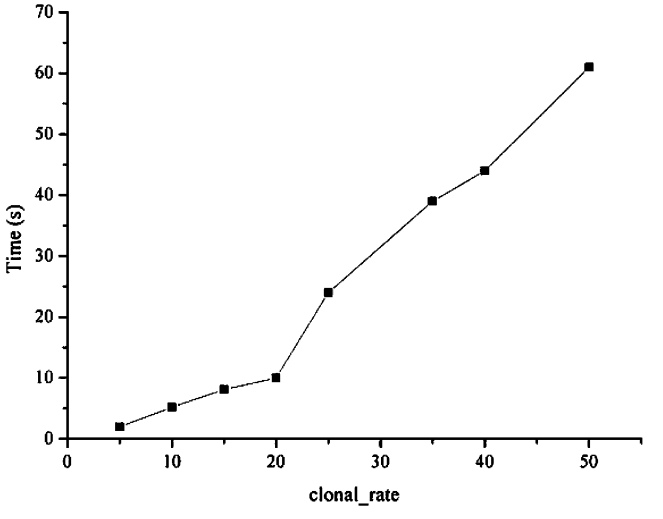

Figure 13. RLCRSI sensitivity in relation to clonal_rate.

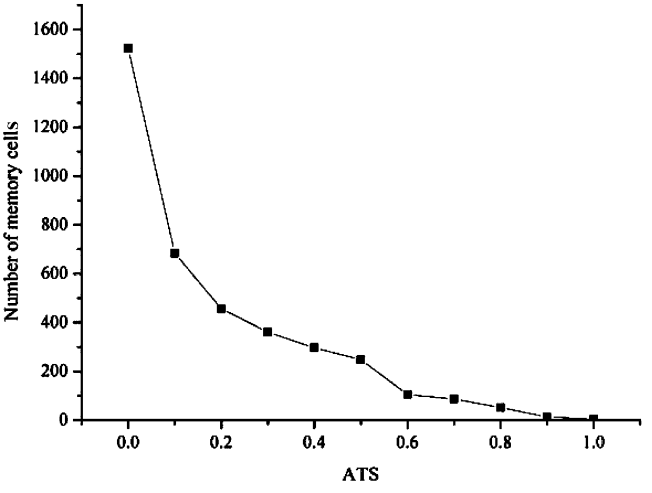

Figure 14. RLCRSI sensitivity in relation to ATS.

experiment 1. The stimulation threshold was assumed with the following values: stimulation threshold = {0.5, 0.6, 0.7, 0.75, 0.8, 0.85, 0.9, 0.95}. As shown in figure 15, the overall accuracy increases from 65% to 92.5% while the stimulation threshold increases from 0.5 to 0.95.

Figure 15 illustrates that the bigger the stimulation threshold, the higher the overall accuracy. The computational cost, however, also increases. In particular, when the stimulation threshold is above 0.85, the overall classification accuracy is only improved from 91% to 92.5%. Therefore, the value of stimulation threshold, 0.9 or 0.85, is often chosen in our practical applications.

6. Conclusions

This paper provides an introduction of AIS in the context of remote sensing classification problems. A novel classifier, RLCRSI, was developed for multi/

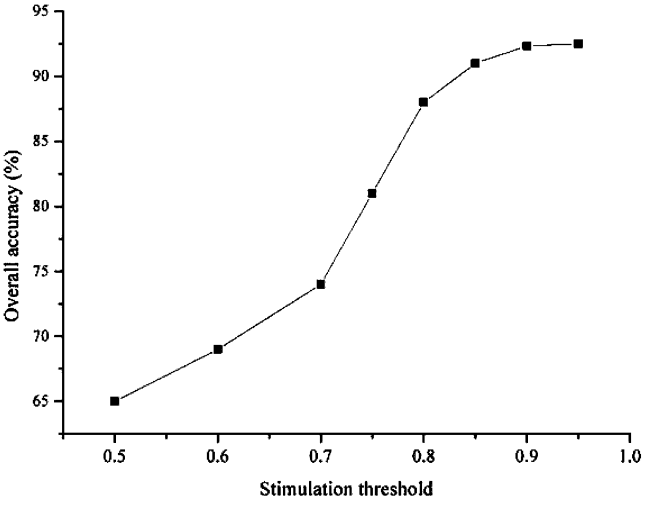

Figure 15. RLCRSI sensitivity in relation to stimulation threshold.

hyper-spectral classification based on the paradigm of improved AIS, i.e. resource limited AIS. RLCRSI is capable of performing data reduction by generating a representative set of memory cells for classification. This set has fewer cells than the original training instances.

A series of experiments were performed to test the performance of RLCRSI using different types of images. Compared to the traditional classifiers, RLCRSI has consistently demonstrated its better performance. In the three experiments, the average classification accuracy was improved from 60% using PP, 87.1% using ML, and 87.91% using BP, to 92.05%; and the Kappa coefficient improved from 0.5418 using PP, 0.8333 using ML, and 0.8444 using BP, to 0.8937 with the acceptable computational cost. This shows that the proposed method is not only suitable for multi/hyper spectral remote sensing image classification, but also proficiently handles high-volume data processing. Consequently, RLCRSI provides an effective option for remote sensing image classification. In our future work, AIS and RLCSRI will be further explored for more extensive remote sensing applications.

Acknowledgements

This work was funded by the 973 Program of the People's Republic of China under grant no. 2003CB415205, the National Natural Science Foundation of China under grant no. 40471088, and the National Science and Engineering Research Council of Canada under grant no. 75-3594. Their support is gratefully acknowledged.

References

CAMPBELL, J.B., 2002, *Introduction to Remote Sensing* (London: Taylor & Francis).

CARPENTER, G.A., GJAJA, M.N., GOPAL, S. and WOODCOCK, C.E., 1997, ART neural networks for remote sensing: Vegetation classification from Landsat TM and terrain data. *IEEE Transactions on Geoscience Remote Sensing*, **35**, pp. 308–325.

CARTER, J.H., 2000, The immune system as a model for pattern recognition and classification. *Journal of the American Medical Informatics Association*, **7**, pp. 28–41.

DASGUPTA, D., 1999, *Artificial Immune Systems and Their Applications* (Germany: Springer).

DE CASTRO, L.N. and TIMMIS, J., 2002, *Artificial Immune systems: A New Computational Intelligence Approach* (London: Springer-Verlag).

DE CASTRO, L.N. and VON ZUBEN, F.J., 2002, Learning and optimization using the clonal selection principle. *IEEE Transactions on Evolutionary Computation*, **6**, pp. 239–250.

DUDA, R.O., HART, P.E. and STORK, D.G., 2001, *Pattern Classification*, 2nd edition (New York: John Wiley & Sons), 517 pp.

FORREST, S., PERELSON, A.S., ALLEN, L. and CHERUKURI, L., 1994, Self-nonself discrimination in a computer. In *Proceedings of the IEEE Symposium on Research in Security and Privacy*, Los Alamitos (CA: IEEE Computer Society Press).

HEERMANN, P.D. and KHAZENIE, N., 1992, Classification of multispectral remote sensing data using a back-propagation neural network. *IEEE Transactions on Geoscience and Remote Sensing*, **30**, pp. 81–88.

JERNE, N.K., 1973, The immune system. *Scientific American*, **229**, pp. 52–60.

KIM, J. and BENTLEY, P., 2001, Towards an artificial immune system for network intrusion detection: An investigation of clonal selection with a negative selection operator. In *Proceedings of the Congress on Evolutionary Computation (CEC)*, Seoul, Korea, **2**, pp. 1244–1252.

LANDGREBE, D.A., 2002, Hyperspectral image data analysis. *IEEE Signal Processing Magazine*, **19**, pp. 17–28.

MICHALEWICZ, Z., 1992, *Genetic Algorithms + Data Structures = Evolution Programs* (New York, NY: Springer-Verlag).

MELGANI, F. and BRUZZONE, L., 2004, Classification of hyperspectral remote sensing images with support vector machines. *IEEE Transactions on Geoscience Remote Sensing*, **42**, pp. 1778–1790.

TARAKANOV, A. and SKORMIN, V., 2002, Pattern recognition by immunocomputing. In *Proceedings of the 2002 Congress on Evolutionary Computation (CEC)*, **1**, pp. 938–943.

TIMMIS, J., NEAL, M. and HUNT, J.E., 2000, An artificial immune system for data analysis. *Biosystem*, **55**, pp. 143–150.

TIMMIS, J., NEAL, M. and HUNT, J.E., 2001, A resource limited artificial immune system for data analysis. *Knowledge Based Systems*, **14**, pp. 121–130.

TSO, B.C.K. and MATHER, P.M., 1999, Classification of multisource remote sensing imagery using a genetic algorithm and Markov random fields. *IEEE Transactions on Geoscience Remote Sensing*, **37**, pp. 1255–1260.

WATKINS, A. and BOGGESS, L., 2002, A resource limited artificial immune classifier. In *Proceedings of the 2002 Congress on Evolutionary Computation (CEC2002)*, Special Session on Artificial Immune Systems (CA: IEEE Press); **1**, pp. 926–931.

ZHANG, L.P., ZHONG, Y.F. and LI, P.X., 2004, Applications of artificial immune systems in remote sensing image classification. In *XXth Congress of International Society for Photogrammetry and Remote Sensing*, Istanbul, Turkey.